J. Fluid Mech. (1973), *vol.* 61, *part* 4, *pp.* 707–730
Printed in Great Britain

Characteristics of the wake behind a cascade of airfoils

By R. RAJ AND B. LAKSHMINARAYANA
Applied Research Laboratory, Pennsylvania State University

(Received 26 February 1973)

An analytical and experimental investigation of the near and far wake characteristics of a cascade of airfoils is reported in this paper. The measurement of mean velocity, turbulence intensity and Reynolds stress across the wake at several distances downstream of the cascade indicates that the wake is asymmetrical and this asymmetry is maintained even up to $\frac{3}{4}$ chord length. Experiments carried out at three incidences reveal that the decay of the wake defect is strongly dependent on the downstream variation of the wake edge velocity. For a cascade, the decay rate of the wake defect is found to be slower than that of a flat plate, cylinder or symmetrical airfoil (at zero incidence). The level of turbulence and Reynolds stresses are found to be high and some comments are made regarding self-preservation and structure of the flow. Semi-theoretical expressions are given for the wake profile, and decay of the velocity defect, turbulence intensity and Reynolds stress.

1. Introduction

The study of the characteristics of the wakes of a cascade of airfoils has a wide range of significant scientific and engineering applications. It has direct application in the aerodynamic design of efficient and compact axial flow compressors, turbines and other types of turbomachinery. Moreover, knowledge of the mean and turbulence properties of a cascade wake are necessary to predict the rotor–stator interaction, the noise generated due to inlet wake and turbulence incidence on a rotating blade row and bending and torsional vibration of the blade row induced by these upstream wakes.

Near and far wakes of a symmetrical airfoil were first investigated experimentally by Silverstein, Katzoff & Bullivant (1939), who provided empirical relationships for the wake decay. Preston & Sweeting (1943) and Preston, Sweeting & Cox (1945) carried out a systematic investigation of the characteristics of the wake behind an isolated airfoil and observed that a similarity in mean velocity profiles exists close behind the airfoil and that the wake centre-line velocity recovers to about 80% of the free-stream velocity within a quarter chord length from the trailing edge. These observations led Spence (1953) to give a general expression of the form

$$1-\frac{U_c}{U_e} = 0{\cdot}1265\left(\frac{x}{c}+0{\cdot}025\right)^{-\frac{1}{2}}, \tag{1}$$

where c is the chord length, U_c the wake centre-line velocity and U_e the wake edge velocity. x is the distance from the trailing edge. According to Spence this

expression holds irrespective of the geometry of the airfoil, which is in doubt. There is at present no general theoretical formulation of wake structure as a function of physical characteristics of an airfoil or its loading. Based on his model equations (Bradshaw, Ferriss & Atwell 1967), Bradshaw (1970) suggested a different type of approach to predict the mean velocity characteristics of the near wake of a symmetrical airfoil using a 'mixing length' fit to data of Chevray & Kovasznay (1969). Bradshaw concluded that the mixing length fit used in the analysis is not valid once the inner wake has spread outside the inner layer of the boundary layer. This type of analysis may not be carried out for the case of asymmetric wakes; the mixing length may be imaginary in part of the flow. In the case of a cascade of cambered airfoils, no analytical treatment, that predicts the wake centre-line velocity, wake width or the turbulence characteristics, is available. Even experimental data are scarce. The only experimental data on mean velocity profiles in a cascade are due to Lieblein & Roudebush (1956); and no conclusion can be drawn from these experiments, because the measurements reported are for a very limited range of cascade flow parameters.

In this paper an effort is made to study systematically, experimentally and theoretically, the near and far wake of a cascade at high Reynolds number (3×10^5). In §3 a flow model, the governing equations and approximate method of solution are proposed for the near and far wake. The experimental set-up and results are discussed in §§4 and 5, respectively. The measured quantities include mean velocity profiles at different incidences, turbulence intensities and Reynolds stress. Criteria and possible regions of self-preservation, the characteristic length and velocity scale are discussed. A general discussion and comparison of the wake of flat-plates, cylinders, isolated and cascade airfoils is also given.

2. Physical nature of cascade wake

A cascade wake is asymmetric. The asymmetry in the wake is due to loading on the airfoil, and the past history of the flow. Far downstream, the wakes of adjacent airfoils in a cascade interact, and the resultant mean velocity profile becomes a periodic function of y with a period S (figure 1). A cascade wake, unlike the wake of an isolated airfoil, encounters an adverse pressure gradient because the edge velocity in it decreases continuously downstream. It differs from the wake of a cylinder, flat plate and an isolated airfoil (symmetrical and cambered), not only in its mean properties, but also in turbulence properties. This subject will be further discussed later.

The characteristics of a cascade wake can be classified and discussed in two categories, depending upon mean and turbulence properties.

(i) *Near wake.* When $U_e - U_c \simeq U_e$ and at the wake centre-line, $\overline{u^2} > \overline{w^2} > \overline{v^2}$. The wake width increases rapidly with streamwise distance downstream of the trailing edge. Here, $\overline{u^2}$, $\overline{w^2}$, $\overline{v^2}$ are the mean turbulence intensities along the x, z, y directions (figure 1). The z co-ordinate is along the blade span.

(ii) *Far wake.* When $U_e - U_c \ll U_e$ (i.e. $(U_e - U_c)^2$ is negligible compared to U_e^2). At the wake centre-line, $\overline{u^2} \simeq \overline{w^2} \simeq \overline{v^2}$. The wake width either becomes constant or increases very slowly.

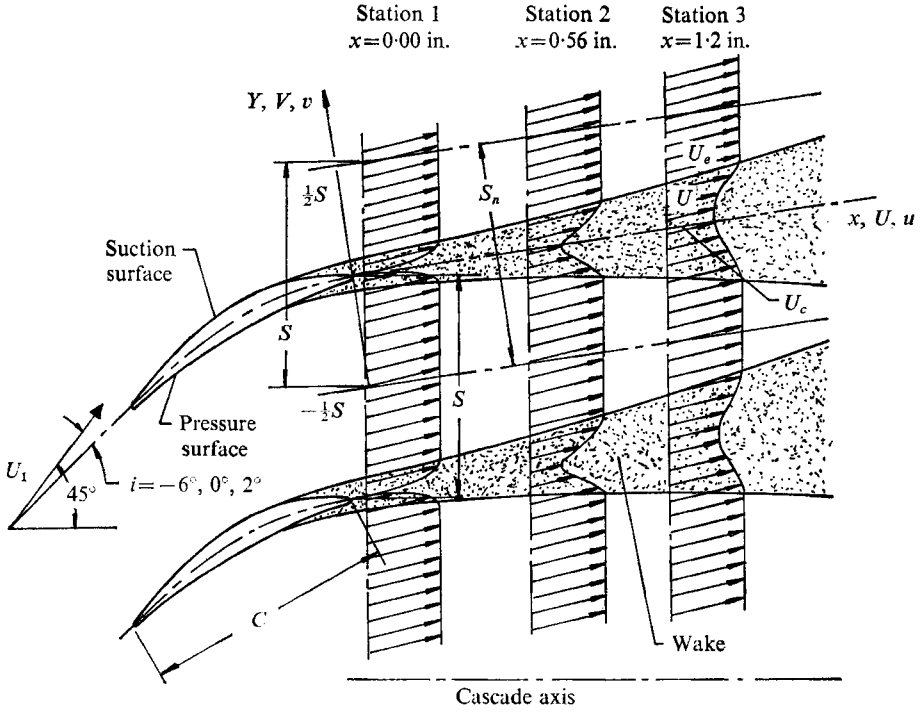

FIGURE 1. Schematic representation of cascade wake development, with notation. Measuring stations: x/c = 0·012, 0·08, 0·16, 0·24, 0·32, 0·40, 0·56 and 0·72.

3. Theoretical considerations

3.1. *Governing equations*

Consider the incompressible flow equations (in tensor notation) of mean motion and Reynolds stress near the trailing edge of the cascade:

$$U_{i,i} = 0, \tag{2}$$

$$\dot{U}_i + U_{i,j}U_j + (\overline{u_i u_j})_{,j} = -p_{,i}/\rho + \nu U_{i,jj}, \tag{3}$$

$$\dot{\overline{u_i u_k}} + U_{i,j}\overline{u_j u_k} + U_{k,j}\overline{u_j u_i} + (\overline{u_i u_k})_{,j}U_j + (\overline{u_i u_k u_j})_{,j}$$
$$= -(\overline{u_k p}_{,i} + \overline{u_i p}_{,k})/\rho + \nu[(\overline{u_i u_k})_{,jj} - 2\overline{u_{k,j}u_{i,j}}], \tag{4}$$

where p, ν, ρ are static pressure, kinematic viscosity and density, respectively, and the superscript dot denotes a time derivative.

The dissipation equation with terms of the order $Re^{-\frac{1}{2}}$ retained (Lumley 1970, 1972) can be written as

$$\dot{\epsilon} + \epsilon_{,j}U_j + \nu(\overline{u_{i,k}u_{i,k}u_j})_{,j} = -4\epsilon^2/q^2, \tag{5}$$

where $q^2 = \overline{u_i u_i}$, $\epsilon = \nu\overline{u_{i,k}u_{i,k}}$.

The terms $(\overline{u_i u_k u_j})_{,j}$, $\nu(\overline{u_{i,k} u_{i,k} u_j})_{,j}$ may be modelled by simple gradient transport, while the deviatoric part of $(\overline{u_k p_{,i}} + \overline{u_i p_{,k}})$ may be expressed as (Lumley 1972)

$$(\overline{u_i u_k} - \tfrac{1}{3} q^2 \delta_{ik}) \frac{1}{T}. \tag{6}$$

The trace of $(\overline{u_k p_{,i}} + \overline{u_i p_{,k}})$ may be included in the gradient transport model of $(\overline{u_i u_k u_j})_{,j}$ (Lumley 1972). Here T is the time scale for return to isotropy and δ_{ik} is the Kronecker delta. T is given by Lumley (1970):

$$T = \frac{1}{8} \frac{q^2}{\epsilon}. \tag{7}$$

Using the above modelling, (4) and (5) can be expressed as

$$\dot{\overline{u_i u_k}} + U_{i,j} \overline{u_j u_k} + U_{k,j} \overline{u_j u_i} + (\overline{u_i u_k})_{,j} U_j - (\overline{u_i u_k})_{,l} \overline{u_l u_j} T)_{,j} + \frac{1}{T} (\overline{u_i u_k} - \tfrac{1}{3} q^2 \delta_{ik}) + \tfrac{2}{3} \epsilon \delta_{ik} = 0, \tag{8}$$

$$\dot{\epsilon} + \epsilon_{,j} U_j - (\epsilon_{,l} \overline{u_l u_j} T)_{,j} = -4\epsilon^2/q^2. \tag{9}$$

For a two-dimensional cascade, (2), (3), (8) and (9) constitute a closed set of eleven equations in eleven unknowns. If it is assumed that the velocity correlation $\overline{uw} \simeq \overline{vw} \ll \overline{uv}$, then the number of equations and unknowns are reduced to nine, and boundary conditions to be satisfied are

$$y = 0, \quad \overline{uv} = 0,$$
$$U = U_e, \quad \overline{uv} = 0.$$

3.2. *Mean velocity profile*

Consider (3) in a two-dimensional Cartesian co-ordinate system. Applying the condition of incompressibility, stationarity, boundary-layer approximation, and neglecting the viscous diffusion and normal stress terms, which are usually small, (3) can be written as (see figure 1 for symbols)

$$U \frac{\partial U}{\partial x} + V \frac{\partial U}{\partial y} + \frac{\partial \overline{uv}}{\partial y} = U_e \frac{\partial U_e}{\partial x}. \tag{10}$$

Assuming self-preservation (experimental results described later confirm this) and using Townsend's (1956) model, the velocity (U_0) and length (L_0) scales are introduced by the relationship

$$U = U_e + U_0 f\left(\frac{y}{L_0}\right). \tag{11}$$

Replace $\overline{uv}$ in (10) with the eddy viscosity model

$$-\overline{uv} = \nu_T \frac{\partial U}{\partial y}. \tag{12}$$

Substitute (11) and (12) in (10) and eliminate V in the resulting equation by the use of the continuity equation (2):

$$\frac{L_0}{U_0}\frac{dU_0}{dx}[f^2]+\frac{L_0}{U_0^2}\frac{d}{dx}(U_eU_0)[f]-\frac{1}{U_0}\frac{d}{dx}(U_eL_0)[\eta f']$$
$$-\frac{1}{U_0}\frac{d}{dx}(U_0L_0)[f']\int_0^\eta f\,d\eta-\frac{\nu_T}{U_0L_0}f''=0, \qquad (13)$$

where $U_0L_0/\nu_T = R_T$ is the Reynolds number and is assumed to be constant.

It is easy to show that the condition of self-similarity in mean velocity profile is satisfied only if coefficients of f, f^2 and f' are constant in (13), i.e. only if

$$\frac{L_0}{U_0}\frac{dU_0}{dx},\quad \frac{L_0}{U_0^2}\frac{d}{dx}(U_eU_0),\quad \frac{1}{U_0}\frac{d}{dx}(U_eL_0)\quad\text{and}\quad \frac{1}{U_0}\frac{d}{dx}(U_0L_0) \qquad (14)$$

are constant.

(i) *Near wake.* When $x/c \simeq 0{\cdot}1$, the first term in (13) is small compared to other terms because the wake centre-line velocity recovers to about 60–70 % (see §5). Furthermore, experimental results (§5) indicate that U_0L_0 is nearly constant in the near wake. Hence, self-similarity is attained if

$$\frac{L_0}{U_0^2}\frac{d}{dx}(U_eU_0)=K_1\quad\text{and}\quad\frac{1}{U_0}\frac{d}{dx}(U_eL_0)=K_2, \qquad (15)$$

where K_1, K_2 are constants. Substituting $U_0L_0 = K_3$ (constant) in (15), we get

$$\frac{1}{U_0^3}\frac{d}{dx}(U_eU_0)=\frac{K_1}{K_3}=K_4 \qquad (16)$$

and

$$\frac{1}{U_0}\frac{d}{dx}\left(\frac{U_e}{U_0}\right)=\frac{K_2}{K_3}=K_5. \qquad (17)$$

Adding (16) and (17) gives

$$U_0\frac{dU_e}{dx}=\tfrac{1}{2}(K_4+K_5)\,U_0^3. \qquad (18)$$

Let $U_e \sim 1/x^m$; then, from (18), we get

$$U_0\sim\frac{1}{x^{\frac{1}{2}(m+1)}}\quad\text{or}\quad\frac{U_0}{U_e}\sim\frac{1}{x^{\frac{1}{2}(1-m)}},\quad L_0\sim x^{\frac{1}{2}(m+1)}. \qquad (19)$$

(*a*) When m is very small ($m \simeq 0$), i.e. U_e is nearly constant,

$$U_0\sim 1/x^{\frac{1}{2}},\quad L_0\sim x^{\frac{1}{2}}.$$

This is the case of a cylinder wake ($x > 100$ diameters), and the case of the near wake of a flat plate, when placed in a uniform stream without pressure gradient.

(*b*) When $m > 0$ (adverse pressure gradient), the wake centre-line velocity will recover more slowly than in case (*a*). This is the case in cascades of airfoils and compressors. If the pressure gradient is large enough ($m > 1$), the wake may grow rather than decay. Hill, Schaub & Senoo (1963) demonstrated this experimentally.

(*c*) When $m < 0$ (favourable pressure gradient), the wake centre-line velocity will recover faster than in case (*a*).

Considering the momentum integral relationship relating the velocity defect in the wake to the profile drag, it can be easily shown that the constant of proportionality in (19) is a function (to first order) of the coefficient of drag ($C_d^{\frac{1}{2}}$) of the cascade of blades.

Thus, a general expression of the form

$$\frac{U_c}{U_e} = 1 - \frac{KC_d^{\frac{1}{2}}}{(x/c + x_0/c)^{\frac{1}{2}(-m+1)}} \tag{20}$$

will predict the wake centre-line velocity recovery in near wakes of cascades of airfoils. The value of K from various experimental data (including that of § 5) is found to be 1·25. x_0/c is the virtual origin. In all practical cases, x_0/c for cascades of airfoils is between 0·02 and 0·03 (Lieblein & Roudebush 1956). Here (§ 5), it is found to be 0·02. Thus, the final expression for the wake centre-line velocity is

$$\frac{U_c}{U_e} = 1 - \frac{1{\cdot}25C_d^{\frac{1}{2}}}{(x/c + 0{\cdot}02)^{\frac{1}{2}(1-m)}}. \tag{21}$$

(ii) *Far wake.* When $U_e - U_c \ll U_e$, the wake width is nearly equal to the spacing(s). Hence, $dL_0/dx \simeq 0$. The pressure gradient effects are also negligible in the case of the far wake of a cascade. Therefore, from (15), we have

$$\frac{L_0}{U_0^2}\frac{d}{dx}(U_e U_0) = K_1 \quad \text{or} \quad U_0 \sim \frac{1}{x}. \tag{22}$$

The constant of proportionality can be evaluated from the momentum integral equation (33), and from the periodic nature of the solution. It can easily be shown that the wake centre-line velocity in this case recovers as

$$\frac{U_c}{U_e} = 1 - \frac{K_6 C_d^{\frac{1}{2}}}{c/S}\left[\frac{1}{x/c}\right], \tag{23}$$

where the constant K_6 depends upon the turbulence characteristics and the wake width. If the spacing and the turbulence characteristics in the far wake of a cascade are similar to those in the far wake of an equally spaced cylinder, then (Schlichting 1968, p. 695)

$$K_6 = \frac{1}{8\pi^3}\left(\frac{S}{l}\right)^2, \tag{24}$$

where l is the mixing length. For low free-stream turbulence ($< 1\,\%$) K_6 is found to be 0·40 (Schlichting 1968).

3.3. *Turbulence quantities*

The turbulence characteristics of the near and far wakes of a cascade are quite different. We shall discuss them separately.

(i) *Near wake.* We shall use (8) to determine the turbulence intensities at the wake centre-line very near the trailing edge of the cascade. Assume that the flow is steady, and the development of flow is confined to a narrow region ($\partial/\partial x \ll \partial/\partial y$). Then the quantities with dots over them vanish. Near the wake centre-line ϵ, $\overline{u^2}$, $\overline{v^2}$, $\overline{w^2}$ (and hence q^2) are nearly constant across the wake. Moreover, $\overline{uv} = 0$,

while dU/dy need not necessarily be zero, but will be small. Using (2), applying these conditions to (8) and rearranging the terms, we get

$$\left.\begin{aligned} U_c\frac{d\overline{u^2}}{dx} &= -\left[\frac{1}{T}\left(\overline{u^2}-\frac{q^2}{3}\right)-\frac{2\epsilon}{3}\right]-2\frac{dU_c}{dx}(\overline{u^2}),\\ U_c\frac{d\overline{v^2}}{dx} &= -\left[\frac{1}{T}\left(\overline{v^2}-\frac{q^2}{3}\right)-\frac{2\epsilon}{3}\right]+2\frac{dU_c}{dx}(\overline{v^2}),\\ U_c\frac{d\overline{w^2}}{dx} &= -\left[\frac{1}{T}\left(\overline{w^2}-\frac{q^2}{3}\right)-\frac{2\epsilon}{3}\right]. \end{aligned}\right\} \tag{25}$$

Qualitatively, (25) suggests that (since dU_c/dx is always positive)

$$\left|\frac{d\overline{v^2}}{dx}\right| < \left|\frac{d\overline{w^2}}{dx}\right| < \left|\frac{d\overline{u^2}}{dx}\right|.$$

Far downstream ($x/c > 1$), the turbulence in a wake tends to be nearly isotropic, i.e. $\overline{u^2} \simeq \overline{w^2} \simeq \overline{v^2}$. If there are no abrupt changes (i.e. the process is continuous from $x/c < 1$ to $x/c > 1$), we conclude that $\overline{v^2} < \overline{w^2} < \overline{u^2}$ near the wake centre-line. Experimentally (§5) it is found that

$$[\overline{u^2}]_{\max}/[\overline{v^2}]_{\max} = 4{\cdot}84. \tag{26}$$

(ii) *Far wake.* In a far wake, the width of the wake becomes equal to the spacing. As a result, the wakes of adjacent airfoils interact, and are no longer separated by the inviscid velocity profile. The peak turbulence intensity and shear stress occur away from the wake centre-line. Therefore, it is not possible to calculate the variation of turbulence intensity at the wake centre-line by the proposed method. However, it is possible to calculate the relative magnitude of the turbulence intensities away from the wake centre-line in the region of maximum shear, where the intensities are nearly independent of y. Since the wake edge velocity is nearly constant far downstream, (8) takes the forms (neglecting $\overline{uw}$ and $\overline{vw}$)

$$2\overline{uv}\frac{\partial U}{\partial y} = -\frac{1}{T}(\overline{u^2}-\tfrac{1}{3}q^2)-2\frac{\epsilon}{3}, \tag{27}$$

$$\overline{u^2}\frac{\partial U}{\partial y} = -\frac{1}{T}\overline{uv}, \tag{28}$$

$$0 = -\frac{1}{T}(\overline{v^2}-\tfrac{1}{3}q^2)-\frac{2\epsilon}{3}, \tag{29}$$

$$0 = -\frac{1}{T}(\overline{w^2}-\tfrac{1}{3}q^2)-\frac{2\epsilon}{3}. \tag{30}$$

It is evident from (29) and (30) that $\overline{v^2} = \overline{w^2}$. Substituting this result and (7) into (29) or (30), it can be shown that $\overline{u^2}/\overline{v^2} = 2$. Similarly, using these results in (27) and (28), it can be shown that $\overline{uv}/\overline{u^2} = 0{\cdot}354$. From the experimental data at $x/c = 0{\cdot}72$ (§5), it is found that

$$[\overline{u^2}]_{\max}/[\overline{v^2}]_{\max} = 2{\cdot}5,$$

and the wake data near the half-wake width indicate that (figure 14)

$$\overline{uv}/\overline{u^2} = 0{\cdot}515.$$

4. Experimental equipment, method and instrumentation

Measurements of mean velocity and turbulence quantities were carried out in a wake region close behind a cascade of blades at various axial and transverse locations (see figure 1). The prime object of these measurements was to study the decay characteristics of mean velocity and turbulence along the streamwise axis, their variation across the wake and their relative order of magnitude.

A subsonic cascade tunnel with porous side walls (for boundary-layer suction), designed and constructed at the Applied Research Laboratory of the Pennsylvania State University, was used in these experiments. The cascade consisted of seven blades of span $l = 14$ in. and chord $c = 7$ in.; it was possible to vary the incidence of the blades. The blade profile used in these experiments is shown in figure 1. The blade profiles are of the loaded-trailing-edge type, and are very similar to the NASA-65 ($8A_2I_{8b}$) 10 blade section.

Mean velocities were measured at an inlet angle $\beta_1 = 45°$, solidity $c/S = 1{\cdot}505$, incidence $i = -6°$, $0°$, $+2°$ (the corresponding flow-turning angles being $22°$, $28°$, $30°$, respectively). The turbulence quantities were measured at only $i = -6°$. The upstream velocity U_1 and turbulence intensity were $80\,\mathrm{ft\,s^{-1}}$ and $0{\cdot}16\,\%$, respectively (see figure 1). Measurements were taken at nine downstream stations ($x/c = 0$, $0{\cdot}012$, $0{\cdot}08$, $0{\cdot}16$, $0{\cdot}24$, $0{\cdot}32$, $0{\cdot}40$, $0{\cdot}56$, $0{\cdot}72$), as shown in figure 1.

Two types of traversing mechanisms were used for measuring the mean velocities (using a five-hole prism-shaped probe) across the wake and turbulence quantities (using a cross-wire probe). Both types of traversing mechanisms had three degrees of freedom: linear motion along x and y axes (figure 1), and rotation of the probe about its own axis.

A five-hole prism-shaped probe was used in combination with three pressure transducers, to measure the resultant direction of the flow and the stagnation and static pressures. The output from the transducers was fed into a data-processing system, to give the desired three quantities. Mean velocity measurements were carried out across the wake at four or five different axial locations (see figure 1).

Two sensor cross-wires, with nearly equal resistance ($R_1 = 10{\cdot}85\,\Omega$, $R_2 = 10{\cdot}84\,\Omega$) and a length to diameter ratio of 250, were used to measure turbulence. No linearizers were used, since the intensity of the turbulence was low. Output from the summing unit was fed to r.m.s. voltmeters, which were connected to digital voltmeters through a three-way key. Measurements were carried out across the wake at eight different axial locations at incidence $-6°$ (see figure 1). The distance between the mounts and the point at which the data were taken was far enough (1 ft) to ensure least interference with the flow.

5. Experimental results and comparison with predictions

5.1. *Mean velocity profile*

As already stated, mean velocity profile measurements in the wake of a cascade were carried out for three incidences ($-6°$, $0°$, $+2°$). The choice of incidence was based on the fact that there was sudden rise in the coefficient of drag beyond the

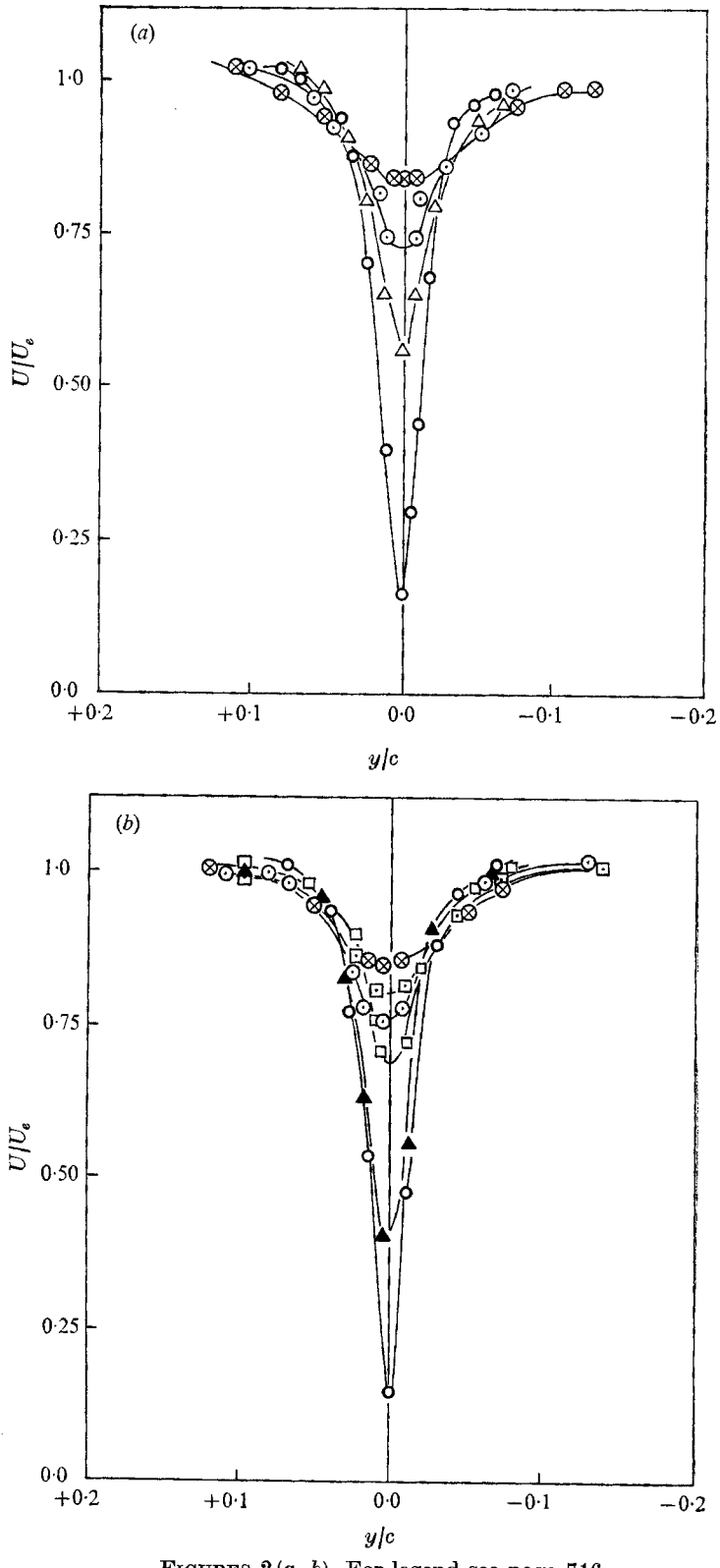

FIGURES 2(*a*, *b*). For legend see page 716.

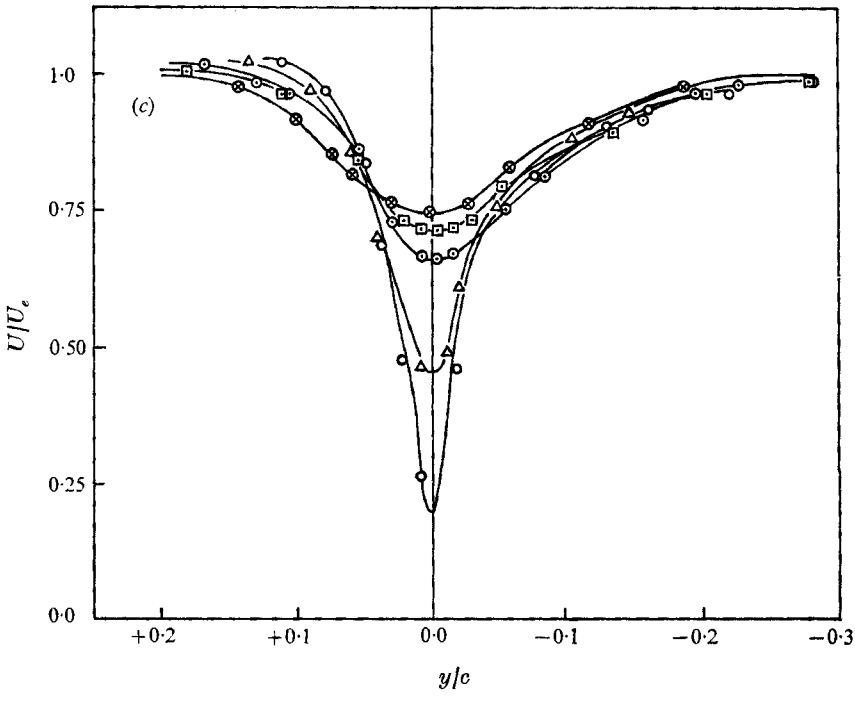

FIGURE 2. Mean velocity profile at (*a*) 0°, (*b*) 2°, (*c*) −6° incidence.

x/c	0	0·012	0·08	0·16	0·24	0·40	0·56
	○	▲	△	□	⊙	⊡	⊗

−6° and +2° incidence for the cascade under investigation. Plots of mean velocity profile across the wake at different axial locations and at different incidences are shown in figures 2 (*a*), (*b*) and (*c*).

At the trailing edge ($x/c = 0{\cdot}0$), the profiles exhibit the characteristics of a boundary layer. The profiles are nearly symmetrical for zero incidence, but show appreciable asymmetry at other incidences (figures 2 (*b*), (*c*)). This asymmetry is preserved even at $x/c = 0{\cdot}56$. The boundary-layer thickness near the trailing edge is greater on the suction surface for incidences $i = 0$ and 2°, and the trend is reversed for incidence $i = -6°$.

(i) *Self-similarity.* In figures 3 (*a*), (*b*) and (*c*) an attempt is made to reduce the mean velocity data to a single curve, using the scaling velocity as the difference between the maximum and minimum velocity ($U_0 = U_e - U_c$), and two different scaling lengths (L_{0s} and L_{0p}), which are distances on the suction and pressure sides of the wake centre-line, from the point of minimum velocity to a point where the velocity is $\frac{1}{2}(U_e - U_c)$.

Figures 3 (*a*), (*b*) and (*c*) show the existence of similarity in velocity profiles, when the velocity and length scales described above are used. The profiles also become symmetrical about the wake centre-line. The mean velocity can be represented by an expression of the type $(1-\eta^{\frac{3}{2}})^2$, where $\eta = y/L_{0s}$ or y/L_{0p}. The length scales L_{0s} and L_{0p} are different in the present case because of the past

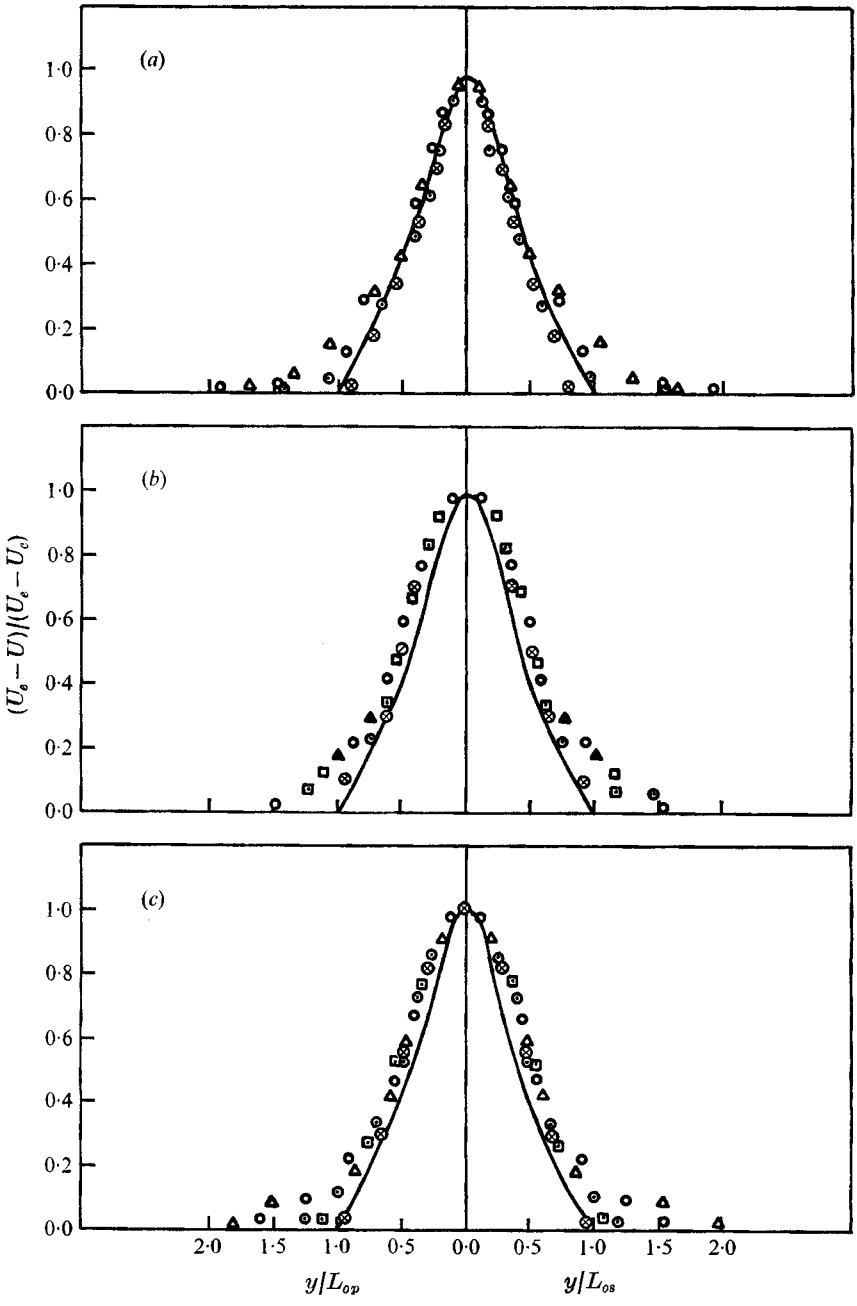

FIGURE 3. Similarity in mean velocity profiles. For symbols see caption to figure 2. ——, $(1-\eta^{\frac{3}{2}})^2$. (*a*) $i = 0°$, (*b*) $i = 2°$, (*c*) $i = -6°$.

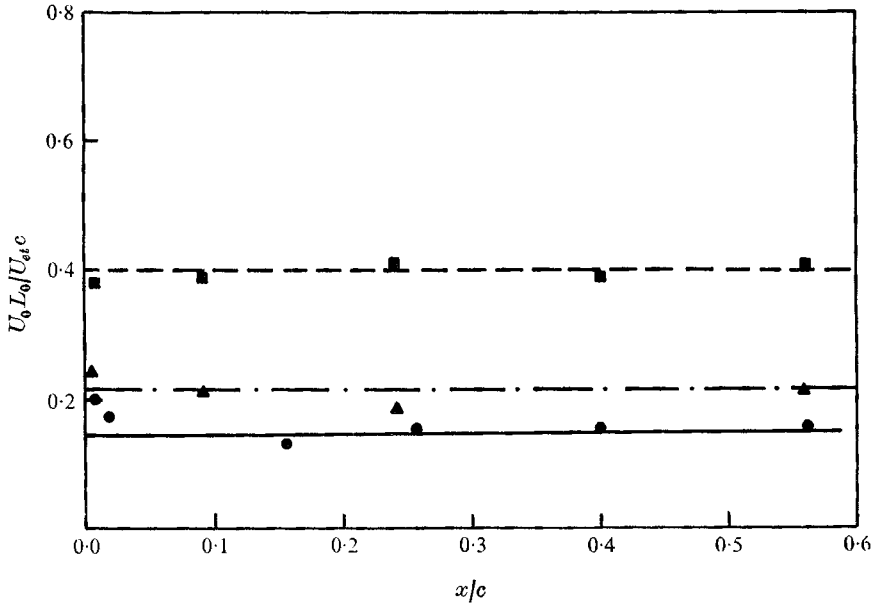

FIGURE 4. Variation of $U_0L_0/U_{et}c$ with downstream distance.
Incidences: ■, $i = -6°$; ▲, 0°; ●, 2°.

history of the flow. However, in the case of the cylinder, flat plate or symmetrical airfoil at zero incidence, $L_{0s} = L_{0p}$.

The ratio $U_0L_0/U_{et}\,c$ is found to be nearly constant at all axial locations and incidences (figure 4). This confirms the self-similarity assumption made in deriving (19).

(ii) *Wake centre-line velocity.* Figures 5 (*a*) and (*b*) show the variation of the wake centre-line velocity with downstream distance at various incidences. Lieblein & Roudebush's (1956) data for a cascade, Chevray & Kovasznay's (1969) data for a flat plate and the data of Preston *et al.* (1945) for an isolated airfoil are shown compared with the authors' cascade data in figure 5 (*a*).

It is clear, from figure 5 (*b*), that the experimental results are in excellent agreement with the theoretical expression (20). Values of K and x_0/c are found to be 1·25 and 0·02, respectively. The values of the coefficients of drag used for determining the constant K in the present investigation are obtained experimentally. In the present investigation, $\frac{1}{2}(-m+1)$ changes from 0·39 to 0·487 for the change in incidence from $-6°$ to $+2°$. It is interesting to note that the value of K reported by Spence (1953) for an isolated airfoil and the authors' for a cascade of airfoils are about the same. While Spence's expression for U_c is valid for zero pressure gradient ($m = 0$), the authors' equation (21) for a cascade is more general.

A few important observations can be made from figure 5 (*a*) about the mean properties of the cascade near wake. (*a*) The wake centre-line velocity is recovered to within 70–80 % between the trailing edge and a position half a chord length downstream. (*b*) The wake of a cascade decays slower than the wake of an isolated airfoil. (*c*) Wake decay of a cascade depends on solidity and incidence.

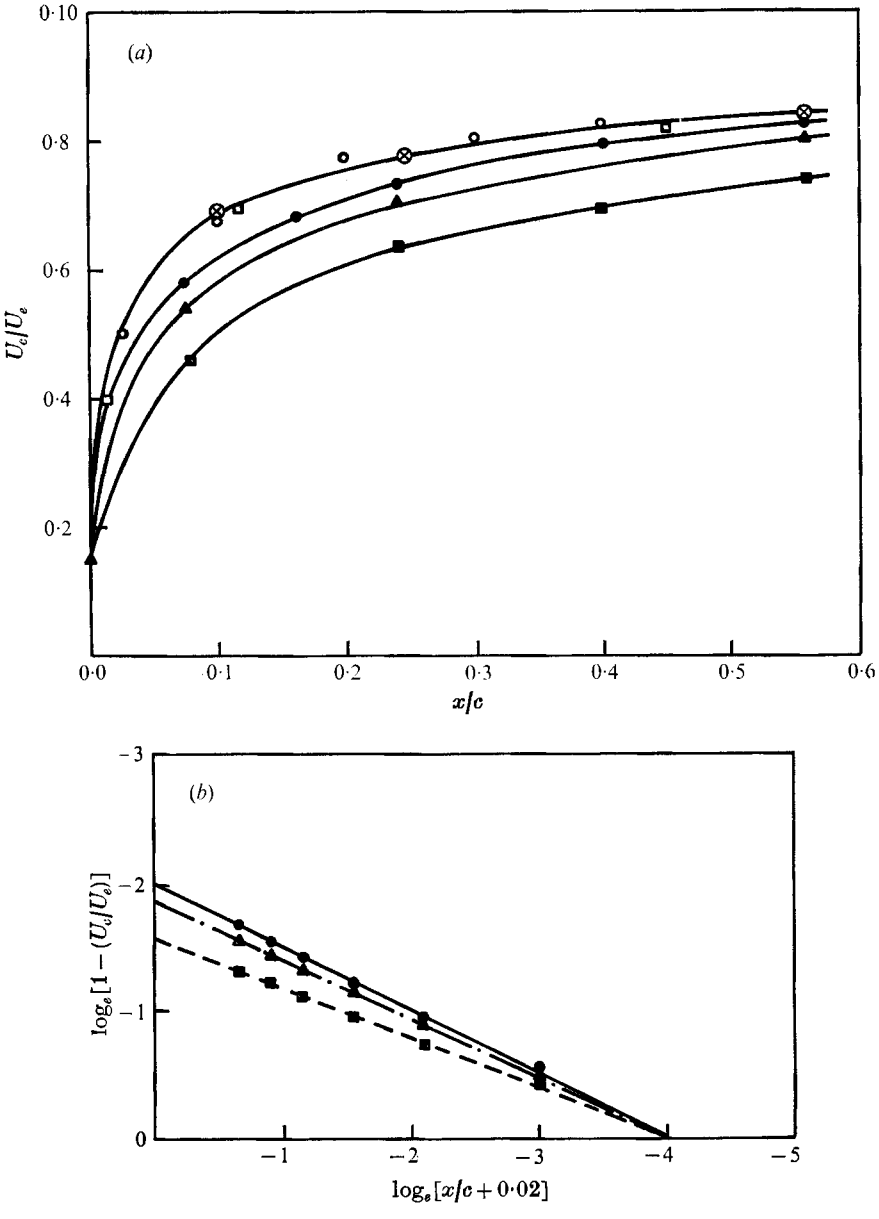

FIGURE 5. Variation of wake centre-line velocity with downstream distance. For incidences see caption to figure 4. Plot (*b*) is logarithmic.

			Equation (20)	$\frac{1}{2}(-m+1)$	C_d
(*a*) ⊗	Isolated airfoil (Preston *et al.* 1945)	(*b*)	———	0·487	0·013
□	Cascade c/s = 0·92 (Lieblein &		—·—	0·45	0·016
	Roudebush 1956)		·····	0·39	0·03
■ ▲ ●	Cascade c/s = 1·505 (authors)				
○	Flat plate (Chevray & Kovasznay 1969)				

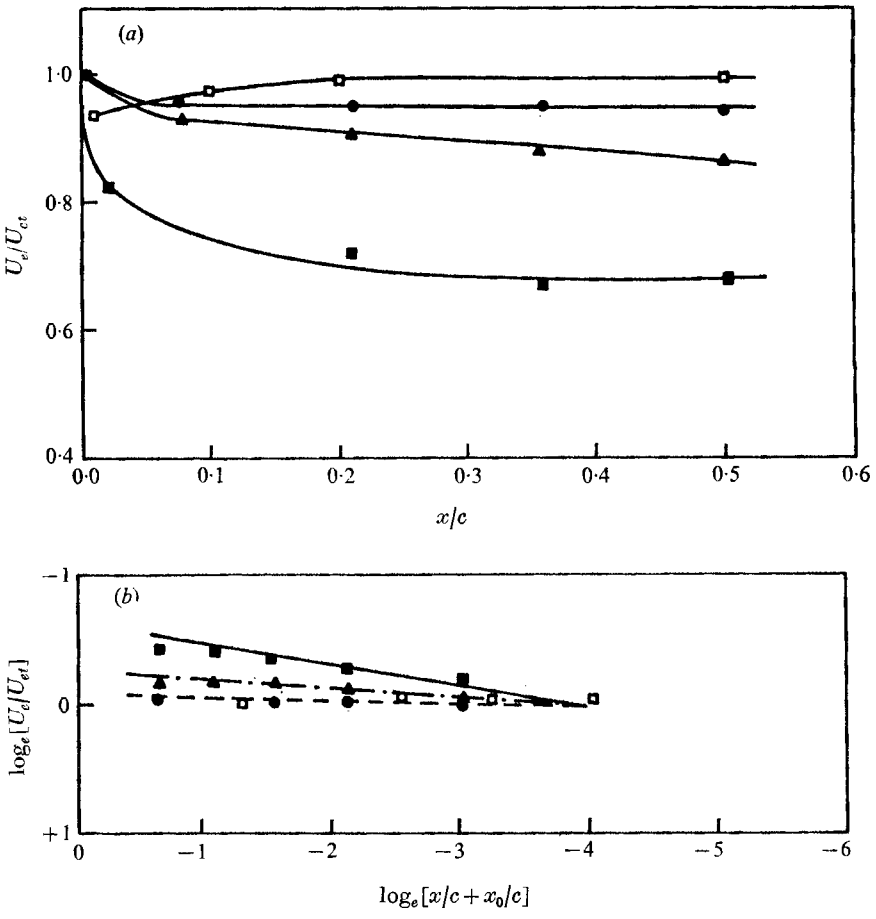

FIGURE 6. Variation of wake edge velocity with downstream distance. For incidences see caption to figure 4. □, isolated airfoil (Preston *et al.*); ■, ▲, ●, cascade (authors). Edge velocity at trailing edge: ——, $U_{et} \sim 1/x^{0\cdot16}$; —·—, $1/x^{0\cdot08}$; – – –, $1/x^{0\cdot03}$.

(*d*) Wake decay of a cascade depends on the geometry of the airfoil used. This is clear from the comparison of the wake of a flat plate and the symmetrical $\frac{12}{40}$ Piercy airfoil (Preston *et al.* 1945) at zero incidence.

No measurements were carried out far downstream ($x/c > 1$). Therefore, it is difficult to comment on the accuracy of (23). However, (23) for $C_d = 1$ reduces to the case of the far wake of an equally spaced row of bars, investigated by Olsson (1936), who showed that there exists good agreement between experimental and theoretical results.

(iii) *Wake edge velocity* U_e. The wake edge velocity measured in the cascade at various incidences is shown plotted and compared with isolated airfoil data in figure 6 (*a*). It is evident that the wake edge velocity for a cascade decreases first very sharply near the trailing edge, then at a much slower rate. This trend is easily explained on the bases of the continuity equation

$$U_{et}(S_n - \delta^*) = \text{const.},$$

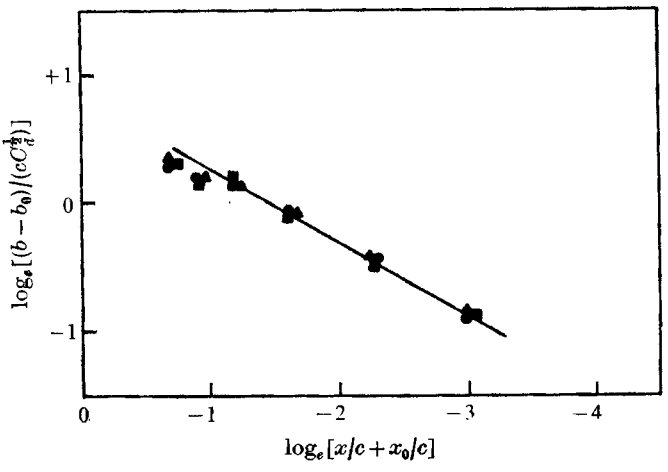

FIGURE 7. Logarithmic plot of variation of wake width with downstream distance. For incidences see caption to figure 4. ——, equation (31).

where U_{et} is the wake edge velocity at the trailing edge, δ^* is the displacement thickness, and S_n is defined in figure 1. δ^* decreases rapidly near the trailing edge, and at a slower rate further downstream. The wake edge velocity for an isolated airfoil increases downstream, while that for a cascade decreases (figure 6 (*a*)).

The edge velocity can be expressed as (figure 6 (*b*))

$$U_e \sim \frac{1}{x^m},$$

where the value of m is found to be $-0{\cdot}028$ for an isolated airfoil and 0·16, 0·08 and 0·03 for a cascade, at incidences $-6°$, 0° and 2°, respectively. Based on this, the exponent of $(x/c+x_0/c)$ in (21) should be 0·42, 0·46 and 0·485 for cascade of blades at $-6°$, 0° and 2°, respectively. Values of this exponent, obtained directly from the wake measurements (figure 5 (*b*)), are found to be 0·39, 0·46 and 0·487, respectively. Thus, the agreement between the theoretically predicted decay rate (20) and the measured rate is good. This clearly indicates the effect of an external pressure gradient ($m \neq 0$), in particular on wake decay.

(iv) *Wake width.* A logarithmic plot of the variation of the wake width at various distances downstream is shown in figure 7. It is interesting to note that most of the wake-width data satisfy the relationship

$$\frac{b-b_0}{cC_d^{\frac{1}{2}}} = 1{\cdot}35(x/c+x_0/c)^{0{\cdot}58}, \tag{31}$$

where b = wake width, b_0 its value at the trailing edge. The values of C_d used in figure 7 are the measured values. The points up to $x/c = 0{\cdot}35$ seem to be well represented by (31), and the exponent in that equation is nearly 0·5 beyond this point.

Theoretically, the exponent in (31) should be 0·58, 0·54 and 0·515 ((19) with $m = 0{\cdot}16$, 0·08 and 0·03) for $-6°$, 0° and 2°, respectively. The discrepancy

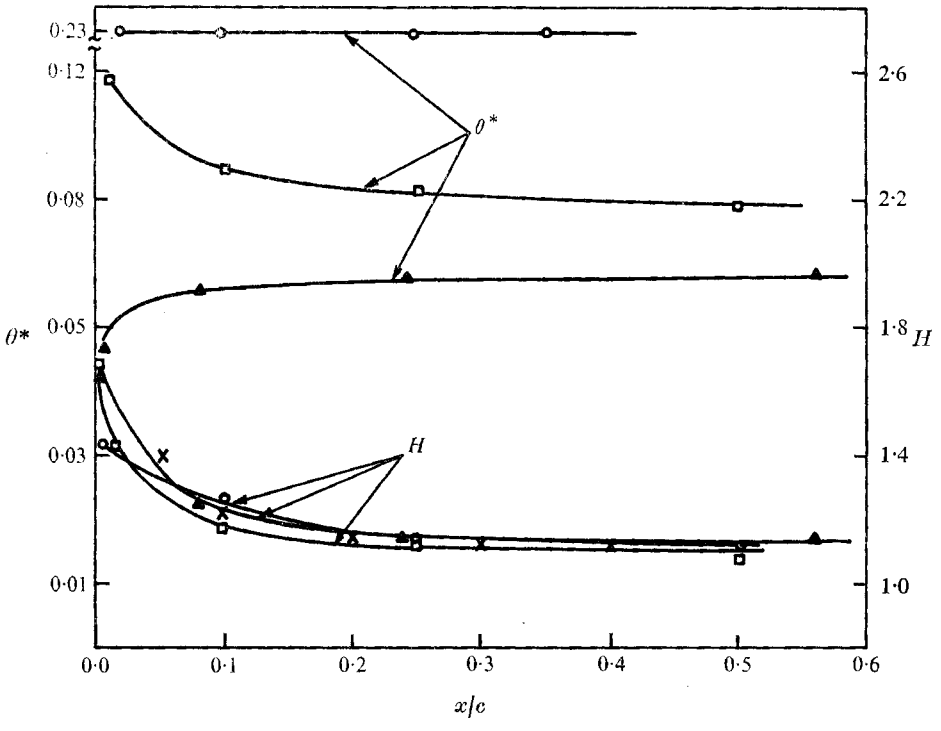

FIGURE 8. Variation of shape factor H and momentum thickness θ^* with downstream distance at incidence 0°. □, isolated airfoil (Preston *et al.* 1945); ○, flat plate (Chevray & Kovasznay 1969); ▲, cascade (authors); ×, equation (34) (predicted).

between theory and experiment may be due to the difficulty in assessing the value of b from the measurements. Nevertheless, it is evident that the widely used representation of wake width ($b \sim x^{\frac{1}{2}}$) is not accurate, especially for a cascade wake with a pressure gradient in the external flow.

(v) *Momentum thickness θ^* and shape factor H.* A plot of the variation of the momentum thickness θ^*, given by

$$\theta^* = \int \frac{U}{U_e}\left(1-\frac{U}{U_e}\right) dy,$$

and the shape factor $H = \delta^*/\theta$ with the downstream distance from the trailing edge is given in figure 8. The magnitude of the momentum thickness first increases, then becomes almost constant, while the shape factor decreases first, then becomes nearly constant. Therefore, the maximum of mixing losses takes place very close to the trailing edge.

The characteristic behaviour of θ^* is explained on the basis of the well-known von Kármán momentum integral equation

$$\frac{d\theta^*}{dx} + (H+2)\frac{\theta^*}{U_e}\frac{dU_e}{dx} = \frac{\tau_0}{\rho U_e^2}. \tag{32}$$

In a wake, skin friction is zero, therefore (32) reduces to

$$\frac{d\theta^*}{dx} + (H+2)\frac{\theta^*}{U_e}\frac{dU_e}{dx} = 0. \tag{33}$$

Equation (33) shows that increase or decrease of θ^* depends on variation of U_e. If U_e increases, then θ^* decreases (isolated), if U_e decreases, then θ^* increases (cascade). This is evident from figure 8.

The variation of the shape factor with downstream distance from the trailing edge of an isolated airfoil was given by Spence (1953):

$$\left(1-\frac{1}{H}\right) = \left(1-\frac{1}{H_t}\right)(40x/c+1)^{-\frac{1}{2}}, \tag{34}$$

where H_t is shape factor at the trailing edge. The same expression accurately predicts the variation of H in a cascade near wake (figure 8).

Since H can be predicted and U_e is known, θ^* for the cascade can be predicted from (34).

5.2. *Turbulence quantities*

(i) *Turbulence intensity.* Figures 9 and 10 plot turbulence intensities in the streamwise ($(\overline{u^2})^{\frac{1}{2}}$) and transverse ($(\overline{v^2})^{\frac{1}{2}}$) directions in a cascade wake at different axial locations. Initially, the curves are asymmetric about the wake centre-line, and the asymmetry is retained in the region of investigation ($0 < x/c < 0{\cdot}72$). The asymmetry about the wake centre-line is due to the past history of the flow. However, far downstream it may disappear, because the flow tries to forget its past history. Maximum turbulence intensity in the present case occurs almost at the wake centre-line. The reasons for this are as follows. Exactly at the wake centre-line, the Reynolds stress is either zero or very small. The anisotropy introduced into the flow owing to the presence of a body is an additional source of turbulence intensity at the wake centre-line. Conversion of mean-flow energy into turbulence energy takes place because of diffusion along the velocity gradients. Transport cannot bring kinetic energy from the centre of the wake, because the gradients of turbulence intensities are negligible there. Therefore energy due to advection and production is completely dissipated there. At the same time, the region of maximum shear close to the wake centre-line will behave in a different way. Because gradients are large, most of the energy transported to the outer part of the wake originates here, while the remainder is dissipated. Hence, it is not unlikely that maximum turbulence intensity will occur at the wake centre-line in the present situation.

However, far downstream of the cascade, maximum turbulence intensity will not usually occur at the wake centre-line, because production due to anisotropy is negligibly small there, and turbulence production peaks (in the region of maximum shear) away from there. Thus, there will be a gradient of the transport of energy to the outer part of the wake; hence, dissipation will be considerably less than in the case of the near wake.

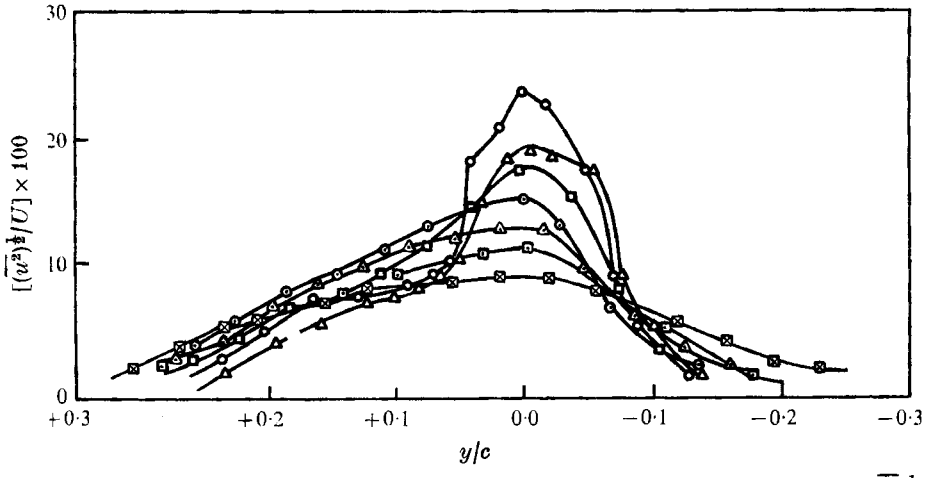

FIGURE 9. Variation of the streamwise component of turbulence intensity ($T_u = (\overline{u^2})^{\frac{1}{2}}/U$) across the wake ($i = -6°$).

x/c	0	0·08	0·16	0·24	0·32	0·40	0·72
	○	△	□	⊙	△	⊡	⊠

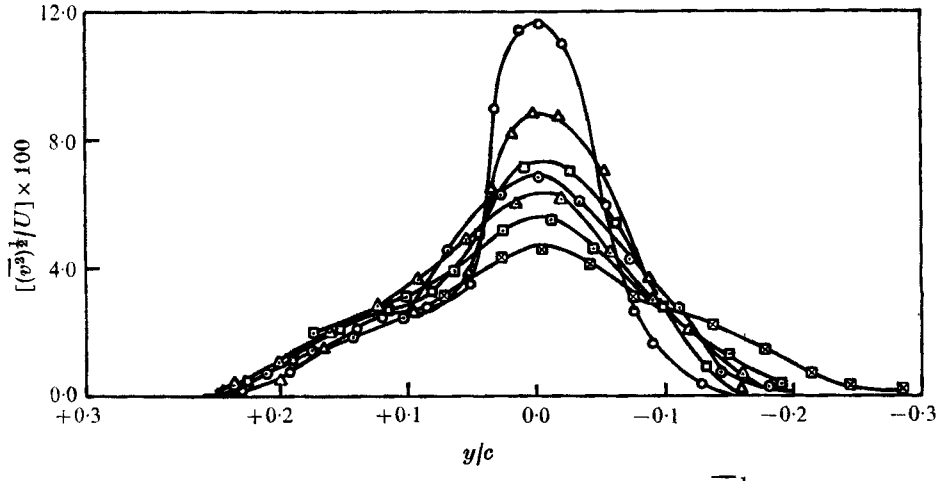

FIGURE 10. Variation of the normal component of intensity ($T_v = (\overline{v^2})^{\frac{1}{2}}/U$) across the wake ($i = -6°$). For symbols see caption to figure 9.

The distance downstream at which the peak of turbulence intensity will no longer occur at the wake centre-line depends on the maximum thickness-to-chord-length ratio in a cascade of slender bodies. For a very thin flat plate, the peak of turbulence intensity may not occur at the wake centre-line, even close to the trailing edge of the plate (Chevray & Kovasznay 1969).

The decay rate of the maximum of $T_u((\overline{u^2})^{\frac{1}{2}}/U)$ and $T_v((\overline{v^2})^{\frac{1}{2}}/U)$ with distance downstream from the trailing edge is shown in figure 12. As is evident from figure 12, $T_{u_{\max}}$ decays faster than $T_{v_{\max}}$ in the region of investigation ($0 < x/c < 0{\cdot}72$). This confirms the earlier conclusion, based on theoretical con-

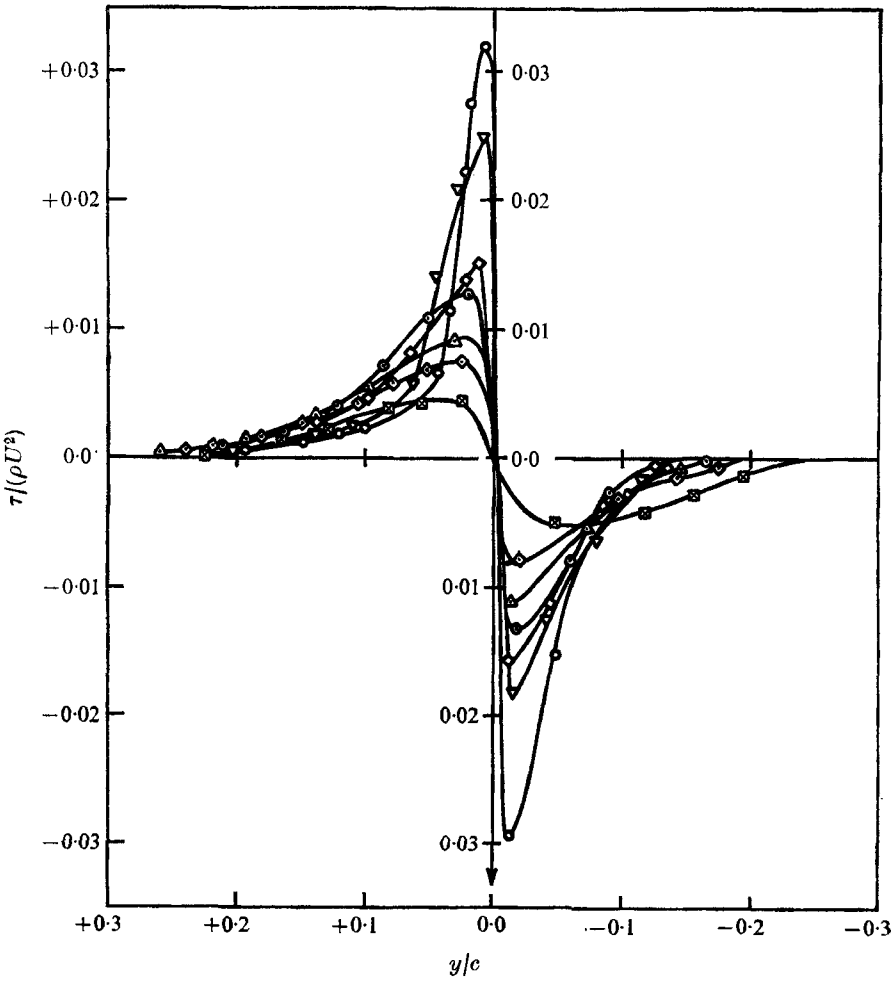

FIGURE 11. Variation of the shear stress $(\tau/\rho U^2)$ across the wake ($i = -6°$).

x/c	0	0·08	0·16	0·24	0·32	0·40	0·72
	○	▽	◇	⊙	△	◇	⊠

siderations of §3.3, (25). The variation of $T_{u_{\max}}$ and $T_{v_{\max}}$ in a cascade can be represented by

$$T_{u_{\max}}\% = 8[x/c + x_0'/c]^{-0.35}, \tag{35}$$

$$T_{v_{\max}}\% = 4{\cdot}6[x/c + x_0'/c]^{-0.20}. \tag{36}$$

All intensities are normalized with respect to local mean velocity. The value of the virtual origin $[x_0'/c]$ in this case is found to be 0·05.

$T_{u_{\max}}$ is found to be roughly twice as great as $T_{v_{\max}}$ near the trailing edge because of wall constraints, as expected. Further downstream, they tend to become equal (figures 9, 10 and 12). The qualitative nature of the behaviour of turbulence intensities at the wake centre-line is consistent with (26). Although the turbulence intensity $(\overline{w^2})^{\frac{1}{2}}$ was not measured, it is predicted that $(\overline{w^2})^{\frac{1}{2}}$ wil

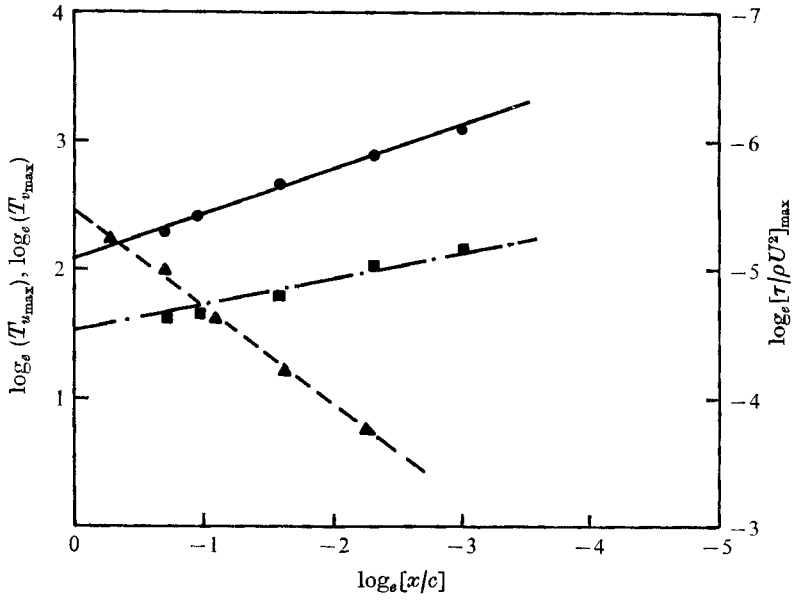

FIGURE 12. Decay characteristics of the maximum turbulence intensities (percentage) and Reynolds stress in the cascade. ●, $T_{u_{max}}$; ■, $T_{v_{max}}$; ▲, $[\tau/\rho U^2]_{max}$. ——, equation (35); —·—, (36); – – –, (37).

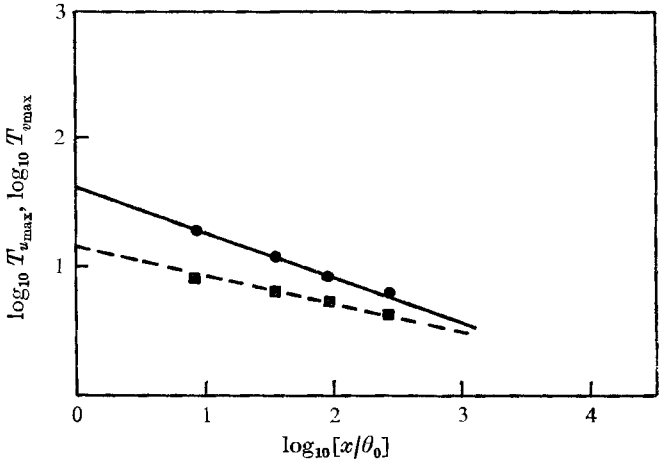

FIGURE 13. Decay characteristics of the maximum turbulence intensities for flat plate (Chevray & Kovasznay 1969). ●, $T_{u_{max}}$%; ■, $T_{v_{max}}$%. ——, $T_{u_{max}} \sim 1/x^{0.344}$; – – –, $T_{v_{max}} \sim 1/x^{0.20}$.

be closer to $(\overline{v^2})^{\frac{1}{2}}$ than to $(\overline{u^2})^{\frac{1}{2}}$. But, away from the trailing edge ($x/c > 0{\cdot}1$), it will take a value intermediate between $(\overline{u^2})^{\frac{1}{2}}$ and $(\overline{v^2})^{\frac{1}{2}}$. $T_{u_{max}}$ and $T_{v_{max}}$ in the case of a flat plate (Chevray & Kovasznay 1969) decay with the same power law as a cascade, i.e. (35) and (36) (see figure 13).

(ii) *Reynolds stress.* Figure 11 shows the distribution of Reynolds stress in a wake behind the cascade at different axial locations. Reynolds stress changes sign

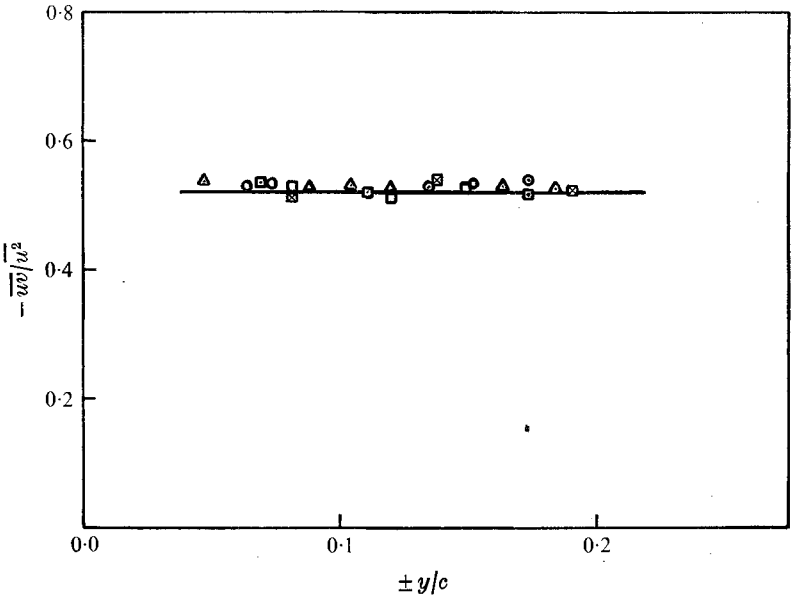

FIGURE 14. Ratio of shear stress to turbulence intensity near half the wake width ($i = -6°$). For symbols see caption to figure 9.

abruptly at the wake centre-line, and maximum shear stress occurs very close to it. Maximum Reynolds stresses on either side of the wake centre-line need not be the same, and are in fact found to be different near the trailing edge (figure 11) of the cascade of cambered airfoils investigated here. However, away from the trailing edge, this difference disappears. The maximum Reynolds stress decreases rapidly along the streamwise direction, up to a distance of $x/c = 0{\cdot}32$ (figure 11). But, for $x/c > 0{\cdot}32$, the rate of decrease is small. Variation of $[\tau/\rho U^2]_{\max}$ with distance downstream is given by (figure 12)

$$\left[\frac{\tau}{\rho U^2}\right]_{\max} = 0{\cdot}005\,[x/c + 0{\cdot}05]^{-0{\cdot}72}. \tag{37}$$

Near the wake centre, the shear stress varies linearly across the wake. A very sound qualitative explanation for such behaviour was given by Townsend (1956) for the far wake. The same reasoning applies also to the near wake. $(\partial\tau/\partial y)_{y=0}$ decreases in the streamwise direction, and the region of maximum shear is displaced away from the wake centre-line with streamwise distance downstream.

In the present investigation, it is found that the point where $\partial U/\partial y = 0$ (the wake centre-line) need not be the same as where the Reynolds stress is zero. This clearly indicates that the mixing length hypothesis is not valid for predicting the mean and turbulence quantities in such a region. The variation of $-\overline{uv}/\overline{u^2}$ with distance downstream from the trailing edge is shown in figure 14, and is found to be constant (0·515) only near the half-wake width. This ratio is not constant across the entire wake. The constant value is found to be a little higher than in flows with uniform distortion of homogeneous turbulence (0·4), or the theoretical value (0·354) predicted in §3.3.

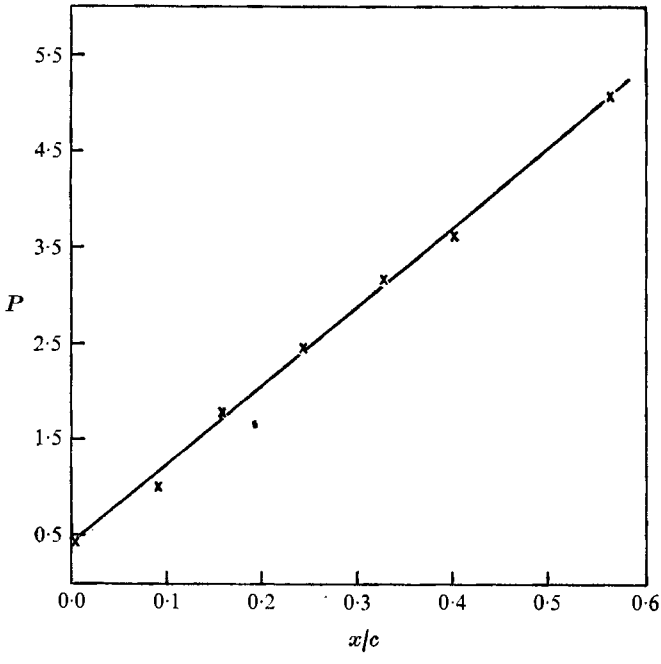

FIGURE 15. Variation of P (equation (39)) with downstream distance.

(iii) *Self-preservation.* An attempt was made to correlate turbulence intensities and Reynolds stress data using the same velocity and length scales as for mean velocity. The data could not be reduced to a single curve as in the case of the mean-velocity profile. This shows that the flow is not completely self-preserved. An understanding of such behaviour can be reached by considering the turbulence-energy equation. In two-dimensional mean motion, the two energy-production terms can be written as

$$-\overline{uv}\frac{\partial U}{\partial y} \quad \text{and} \quad (\overline{u^2}-\overline{v^2})\frac{\partial U}{\partial x}. \tag{38}$$

The first of these is usually ignored in homogeneous, distorted turbulence, while the second occurs in the description of an isotropic far wake. Therefore, the term introducing non-self-preservation into the flow is the second. Since at the trailing edge of the cascade there is production of turbulence intensity and the flow is anisotropic, the second term is of comparable magnitude to the first term. The production of turbulent energy differs for various bodies, and depends on the shape of the body. In the case of bluff bodies, the second term is of a much higher order (three or four times) than in the case of a streamlined body or a flat plate. This is the reason why, in the case of a streamlined body, self-preservation is attained much earlier than in the case of bluff bodies. Reynolds (1962), using the above two energy-production terms, deduced a criterion for self-preservation:

$$P = \left[\frac{-\overline{uv}\,\partial U/\partial y}{(\overline{u^2}-\overline{v^2})\,\partial U/\partial x}\right]_{y=L_0}, \tag{39}$$

where L_0 is half the wake width. If $P > 1$ (i.e. in shear-dominated flows), the flow tends to be nearly self-preserved. But for complete self-preservation, P must have a much greater value ($\geqslant 10$). If $P < 1$, the flow is not self-preserved. Variation of P downstream in the streamwise direction of the cascade is shown in figure 15. This shows that from $x/c \simeq 0{\cdot}24$ onwards the wake is nearly self-preserved. It is interesting to note that P varies linearly with distance downstream in the near wake.

6. Discussion and conclusion

The experimental and analytical investigations reported in this paper indicate that the wake of a cascade of airfoils differs from that of a cylinder, flat plate or isolated (symmetrical) airfoil at zero incidence, in several respects.

(i) The wake is asymmetrical. When two different length scales are used, one for each side of the wake, mean velocity profiles become symmetrical about the wake centre-line.

(ii) The wake edge velocity changes continuously, giving rise to either slower decay of the wake defect (as in the case of a cascade with decelerating free-stream flow) or faster decay (as in the case of accelerating mean flow). The mean velocity profile is of the type $(1-\eta^{\frac{3}{2}})^2$, where $\eta = y/L_{0s}$ or y/L_{0p}, and L_{0s}, L_{0p} are length scales on the suction and pressure side of the wake, respectively. The wake centre-line velocity is well represented by (21), and the width of the wake by (31).

(iii) Turbulence intensities are higher than those of a flat-plate wake, even though decay characteristics ((35) and (36)) are nearly the same. Maximum Reynolds stress and decay characteristics are given by (37).

The change in cascade parameters (e.g. solidity c/S and incidence i) has a dual effect. Solidity is likely to change the wake edge velocity (m in the equation $U_e \sim x^{-m}$) and the profile drag. Both of these change the wake decay characteristics. But in the far wake, where $U_e \sim$ const., the velocity defect at the wake centre-line is inversely proportional to solidity (see (23)). The incidence and camber effects (which directly control boundary-layer growth, blade loading and drag coefficient) would similarly influence the decay rate through the parameters C_d and m. The results reported here adequately demonstrate this.

Schlichting (1968, p. 695), while investigating the far wake of a cascade of circular cylinders, derived a theoretical expression for the mean velocity, which shows no dependency on C_d. This is due to the fact that the C_d for a circular cylinder in the Reynolds number range of 10^4–10^5 is nearly unity, while that of a cascade of blades is two or three orders of magnitude less.

The peak in turbulence intensity may occur at the wake centre-line in a cascade, depending on the thickness of the blade and the downstream distances. Experimental data of Reynolds (1962) show a similar trend. For large-diameter cylinders, the interaction of the mean-velocity defect and the turbulence intensity is delayed, resulting in the occurrence of the turbulence peak at the wake centre-line. However, the turbulence intensity peak will be away from the wake centre-line for the same cylinder at larger downstream distances.

No attempt is made in this paper to investigate the effect of inlet turbulence.

At higher levels of free-stream turbulence, the wake decay characteristics may be different (Eagleson, Huval & Perkins 1961). The data of Eagleson *et al.* for a flat-plate wake in a water tunnel indicate that the near-wake decay law changes from $x^{-\frac{1}{2}}$ to x^{-1} when the turbulence level is around 4–7 %. This is an area where further research is needed.

The authors wish to express their gratitude to Dr John Lumley for many helpful discussions on the theoretical model and to Mr Jack Ross for his help in the experimental set-up. This work was sponsored by the Applied Research Laboratory of the Pennsylvania State University, which operates under contract with the Naval Ordnance Systems Command.

REFERENCES

Bradshaw, P. 1970 *A.I.A.A. J.* **8**, 1507.

Bradshaw, P., Ferris, D. H. & Atwell, N. P. 1967 *J. Fluid Mech.* **28**, 593.

Chevray, R. & Kovasznay, S. G. 1969 *A.I.A.A. J.* **7**, 1641.

Eagleson, P. S., Huval, C. J. & Perkins, F. E. 1961 *M.I.T. Hydrodynamics Lab. TR* no. 46.

Hill, P. G., Schaub, U. W. & Senoo, Y. 1963 *Trans. A.S.M.E.* E **30**, 518.

Lieblein, S. & Roudebush, W. H. 1956 *N.A.S.A. Tech. Note* no. 3771.

Lumley, J. L. 1970 *J. Fluid Mech.* **41**, 413.

Lumley, J. L. 1972 *Int. Symp. on Stratified Flows*, Novosibirsk.

Olsson, R. G. 1936 *Z. angew. Math. Mech.* **16**, 257.

Preston, J. H. & Sweeting, N. E. 1943 *Aero. Res. Counc. R. & M.* no. 1998.

Preston, J. H., Sweeting, N. E. & Cox, D. K. 1945 *Aero. Res. Counc. R. & M.* no. 2013.

Reynolds, A. J. 1962 *J. Fluid Mech.* **13**, 333.

Schlichting, H. 1968 *Boundary Layer Theory*. McGraw-Hill.

Silverstein, A., Katzoff, S. & Bullivant, W. 1939 *N.A.S.A. Rep.* no. 651.

Spence, D. A. 1953 *Aero. Res. Counc. C.P.* no. 125.

Townsend, A. A. 1956 *The Structure of Turbulent Shear Flow*. Cambridge University Press.